Antibacterial activity of flame-made Ag/SiO_2 nanoparticles

[1]Georgios A. Sotiriou, [1]Adrian Camenzind,
[2]Andreas Meyer, [2]Sven Panke and [1]Sotiris E. Pratsinis

[1]Particle Technology Laboratory, [2]Bioprocess Laboratory, Institute of Process Engineering
Department of Mechanical and Process Engineering
Swiss Federal Institute of Technology
Zurich (ETH Zurich)

ABSTRACT

Silver (Ag) nanoparticles dispersed in an amorphous silica (SiO_2) matrix were synthesized by flame spray pyrolysis (FSP). Three different precursor solutions were used for the flame synthesis of the nanoparticles. The morphology of the produced particles was investigated. Additionally, the antibacterial activity of the synthesized particles was monitored against the Gram negative bacteria *Escherichia coli*. The amount of Ag surface area which is exposed (*Ag SSA*) depends on the precursor selection. The antibacterial activity is enhanced for an increased Ag content, as expected. This activity was correlated to the *Ag SSA*, showing that the mechanism responsible for the antibacterial properties is strongly surface area dependent.

Keywords: silver, silica, nanoparticles, antibacterial, SSA

1 INTRODUCTION

Silver's ability to kill microorganisms is known for many years. The mechanism responsible for silver's antibacterial ability is not yet fully understood. Feng *et al.* [1] investigated the effect of Ag^+ ions on bacterial cells and concluded that Ag^+ ions interfere with DNA replication. Morones *et al.* [2] investigated the activity of silver nanoparticles against bacteria and proposed that silver nanoparticles damage the integrity of the cell membrane and may penetrate into the interior. In doing so, they interact with and possibly destroy sulfur or phosphorus containing compounds (such as DNA) that are vital for the cell. Furthermore, Morones and coworkers suggest that the Ag nanoparticles release Ag^+ ions from their surface, contributing additionally to the antibacterial properties. Lok *et al.* [3] found that the parameter that affects silver's antibacterial property is the Ag^+ ions which is chemisorbed on the surface of the metallic silver nanoparticles. Zero-valent silver nanoparticles have no antibacterial activity, while the partially surface oxidized silver nanoparticles exhibit antibacterial activity due to the chemisorbed Ag^+ ions on their surface. However, whenever Ag nanoparticles are dispersed in a high salt content solution they tend to aggregate, losing their high antibacterial activity [3].

One way to stabilize the Ag nanoparticles is to attach them on a support material, such as silica (SiO_2). Most methods for the synthesis of Ag/SiO_2 nanocomposites involve wet phase synthetic routes, with the most well known the sol-gel method [4]. However, most of the wet synthetic routes are time-consuming, they involve multiple steps processes, and there are limitations in the scalability [5].

Flame synthesis is one of the established commercial processes for making inexpensive ceramic nanoparticles [6]. Recently, flame spray pyrolysis (FSP) has been developed, with which liquid precursor solutions are used and the synthesis of a broad range of products including metal oxides, mixed metal oxides and metals on metal oxides is possible [7]. The synthesis of Ag nanoparticles doped on ZnO for photocatalytic applications has been reported with FSP [8]. Additionally, Ag/SiO_2 nanoparticles have been produced by FSP, and their catalytic activity was tested, as well as their antimicrobial and antifungal properties [9, 10]. However, there has not been any study investigating the precursor selection effects on the morphology of the product particles, as well as the correlation between the Ag content and the antibacterial activity.

2 EXPERIMENTAL

Three different precursor solutions were used for the production of the Ag nanoparticles dispersed in SiO_2. For all the precursor solutions, the appropriate amounts of the Ag precursor were dissolved in the selected solvents, and prior to their introduction into the FSP setup, appropriate amount of the SiO_2 precursor was added and stirred. For the first precursor solution, Ag nitrate (Fluka, purity >99%) was dissolved at room temperature in ethanol (Alcosuisse, purity >98%) and diethylene glycolmonobutyl ether (Fluka, purity >98%) with a volume ratio of 1:1, with hexamethyldisiloxane (HMDSO, Aldrich, purity >97%) as the SiO_2 precursor. Ag acetate (Aldrich, purity >99%) dissolved in 2-ethylhexanoic acid (2-EHA, Fluka, purity >98%) and toluene (Fluka, purity >98%) with a volume ratio 1:1 at 140°C and HMDSO (Aldrich, purity >97%), were the components of the second precursor solution. Ag nitrate dissolved in 2-propanol (Fluka, purity >98%) at 90°C, and tetraethyl orthosilicate (TEOS, Aldrich, purity >98%) were used as the Ag and SiO_2 precursors for the third precursor solution. For all the three precursor solutions, the total metal (Ag and Si) concentration was

NSTI-Nanotech 2009, www.nsti.org, ISBN 978-1-4398-1783-4 Vol. 2, 2009

kept at 0.5 M. The weight fraction of the Ag in the product was defined as follows:

$$wt\%Ag = \frac{mass(Ag)}{mass(Ag) + mass(SiO_2)} \times 100$$

and ranged from 0 – 25 wt%. The notation for the different particle concentrations which will be adopted from now on is: *xAg/SiO₂*, for a concentration of *x wt%* of Ag in the final product. The combustion enthalpy density was defined as the ratio of the fed liquid precursor combustion enthalpy (kJ/min), over the total gas flow (g_{gas}/min) within the spray [11].

The particle synthesis was carried out using a flame spray pyrolysis (FSP) reactor which is described in detail elsewhere [7]. The produced particles were characterized by TEM/STEM (FEI; LaB6 cathode, operated at 300 kV, point resolution ~2 Å) and EDAX analysis (EDXS; detector (EDAX) attached to the Tecnai F30 microscope), X-ray diffraction (Bruker AXS D8 Advance spectrometer (Cu Kα, 40 kV, 40 mA). The specific surface area (*SSA*) of the samples was measured by five-point nitrogen adsorption at 77 K (BET: Micrometrics Tristar 3000) after degassing the samples at 150 °C for 1.5 hours in nitrogen. The exposed surface area of Ag (notation which will be used from now on: *Ag* SSA_{EXP}) was measured with O_2 pulse chemisorption with a Micromeritics Autochem II 2920 unit.

To examine the antibacterial effect of the samples a growth inhibition assay was performed. To do so, *E. coli* JM101 bacteria synthesizing a green fluorescent protein (GFP) from a plasmid-encoded gene were grown in Luria-Bertani broth (LB) [12] at 37 °C overnight. The culture was subsequently diluted with LB to an optical density (OD) at 600 nm of 0.05, which corresponds to approximately 10^7 colony forming units (CFU)/ml. The Ag/SiO_2 nanoparticles were dispersed in de-ionized water using ultrasonication (Sonics vibra-cell) for 20 seconds at 50% amplitude, with a pulse configuration on/off of 0.5s/0.5s. After ultrasonication, the nanoparticles were homogeneously dispersed and stable in the aqueous solution. For the assay, 50 µl of the aqueous solutions containing the dispersed Ag/SiO_2 nanoparticles were added to 50 µl of the diluted cells in a 96 well plate. The growth of *E. coli* JM101 was assessed by monitoring the fluorescent signal of the GFP (Perkin Elmer 1420). For analysis of the data the values were corrected for the initial background fluorescence. The error bars for each data point were obtained as the standard deviation of 4 measurements.

3 RESULTS & DISCUSSION

3.1 Particle morphology

Flame spray pyrolysis (FSP) of the Ag/SiO_2 precursor solutions resulted in the formation of Ag nanoparticles which were dispersed in an amorphous SiO_2 matrix. In Figure 1 one STEM image of the produced sample *1Ag/SiO₂* resulting from the precursor solution containing Ag acetate-HMDSO and its corresponding EDX spectra are shown. The EDX spectra below each STEM image give the elemental composition signal at the area where the electron beam is focused. From the EDX data it can be seen that the materials that compose the produced sample are Ag and SiO_2. For the spectrum 1, the beam is focused on a bright area which corresponds to a single Ag nanoparticle, since the appearing peaks are attributed only to Ag. For the spectrum 2, the electron beam is focused on the diffuse grey area, which corresponds to the amorphous SiO_2, since peaks of Si and O are present in the EDX spectrum. Should any Ag oxide be present in the final product, a peak corresponding to O would have appeared also to the EDX spectrum 1. The peaks which correspond to C and Cu are due to the perforated carbon foil supported on a copper grid which was used to obtain the TEM/STEM images. Similar results from the EDX analysis were obtained for the three produced samples resulting from the different precursor solutions. Therefore, it can be concluded that the composition of the produced nanoparticles, within the detection limit of the EDX, does not depend on the precursor selection, since metallic Ag and SiO_2 are produced from all the precursors.

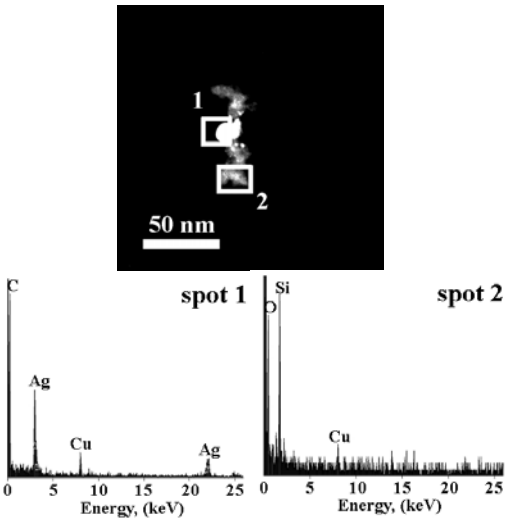

Figure 1: STEM image of the *1Ag/SiO₂* produced sample resulting from the Ag acetate-HMDSO precursor solution. Below the STEM image the EDX spectra are shown which correspond to the areas where the electron beam is set.

The effects on the morphology of the produced samples from the precursor selection can also be seen from the STEM and TEM images. In Figure 2, two STEM images (a, b) are shown from the two *10Ag/SiO₂* samples, resulting from the Ag nitrate-HMDSO and Ag acetate-HMDSO precursor solutions, respectively. The STEM images reveal that the Ag particles (bright areas) are well dispersed in the amorphous SiO_2 matrix (diffuse gray) in both samples. It can also be observed that there is a broad range of detected

Ag particle sizes. However, for the sample produced from the Ag nitrate precursor, it can be seen that this inhomogeneity is more pronounced, since even big particles in the range of ~150 nm are observed. The sample produced from the Ag acetate precursor does not have these bigger particles and, thus, there is a higher particle homogeneity.

The observed inhomogeneity in image (a) could be attributed to the precursor components. It has been reported that the parameters that affect the homogeneity of the produced particles during flame synthesis are the combustion enthalpy density and the ratio of the boiling point of the solvent over the decomposition point of the precursor (T_{bp}/T_{dp}). There is a trend for homogeneity for higher combustion enthalpy densities, as well as for higher values of the above mentioned ratio [11]. The combustion enthalpy density of the precursor containing Ag acetate is higher than the one of the precursor containing Ag nitrate (0-25 wt% of Ag; Ag nitrate-HMDSO: 7.7 – 8.1 kJ/g_{gas}, Ag acetate-HMDSO: 8.6 – 8.9 kJ/g_{gas}). Additionally, the values of the ratio T_{bp}/T_{dp} for the two different precursor solutions are 0.9 and 0.6, respectively. Therefore, it can be concluded that the higher homogeneity which is observed from the STEM image (b), could be attributed to the precursor composition.

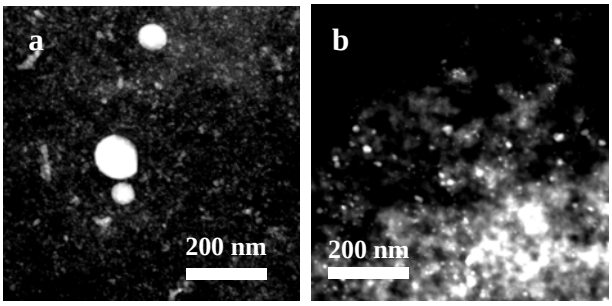

Figure 2: STEM images of the *10Ag/SiO₂* resulting from the precursor solution containing Ag nitrate-HMDSO (a), and resulting from the precursor solution containing Ag acetate-HMDSO (b).

With O_2 chemisorption it is possible to detect the Ag surface area which is exposed [13]. In Table 1, the measured *Ag* SSA_{EXP} of the nanoparticles resulting from the different precursor solutions is presented. For the low Ag content, the error bar (coming from 4 different measurements, as the standard deviation of the data points) is comparable to the measured values, therefore it would not be safe to draw quantitative conclusions; however, for all three samples resulting from the different precursor solutions, it is evident that there are higher values of the *Ag* SSA_{EXP} for higher Ag content. It is noticeable that the highest values are obtained for the particles resulting from the Ag nitrate-TEOS precursor solution, while the ones from the Ag acetate-HMDSO have the lower values. This could be attributed to the partial embedding of the Ag nanoparticles within the SiO_2. In case Ag acetate is used as precursor, the Ag nanoparticles are more embedded within the SiO_2 matrix, than in case Ag nitrate is used. The reason for this fact could be due to the lower decomposition point that Ag acetate has, in comparison to the Ag nitrate. When precursors with lower decomposition points are used, the Ag formation starts earlier, along with the formation of SiO_2, having as a result the embedding of the Ag nanoparticles with SiO_2.

Sample	Precursors	*Ag* SSA_{EXP} (m^2/g)	Deviation (± m^2/g)
1Ag/SiO₂	*Ag nitrate-HMDSO*	0.20	0.11
6Ag/SiO₂		0.64	
10 Ag/SiO₂		0.85	0.12
25 Ag/SiO₂		1.27	0.11
1 Ag/SiO₂	*Ag nitrate-TEOS*	0.16	
6Ag/SiO₂		0.73	
10 Ag/SiO₂		1.15	
25 Ag/SiO₂		1.60	0.13
1 Ag/SiO₂	*Ag acetate-HMDSO*	0.25	
6Ag/SiO₂		0.32	
10 Ag/SiO₂		0.56	
25 Ag/SiO₂		0.63	0.12

Table 1: The values of the *Ag* SSA_{EXP} for all the produced samples, as well as the standard deviation indicating the error bar of the measurements.

3.2 Antibacterial activity

The antibacterial effect of the samples produced from the precursor solution containing Ag nitrate-HMDSO was examined against the Gram-negative bacterium *E. coli*.

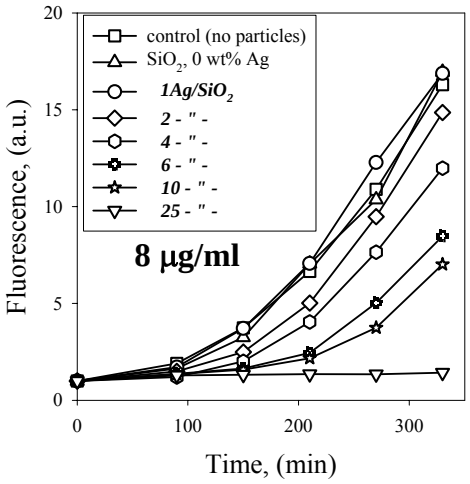

Figure 3: Growth curves of *E. coli* JM101 in the presence of different Ag content particles (0-25 wt %) at a particle concentration of 8 μg/ml.

In Figure 3, the fluorescence of *E. coli* cultures synthesizing GFP at 37°C in the presence of the Ag/SiO_2 nanoparticles is presented as a function of time,

representing the growth of the strain under the different experimental conditions. Figure 3 shows the results from the investigation of the effect of the Ag content (0-25 wt %), keeping the particle concentration constant (8 μg/ml). It can be seen that pure SiO_2 particles do not affect the growth of the bacteria. However, in the presence of the Ag-containing SiO_2 particles, the antibacterial effect is increased with an increased Ag content. No growth at all after 5.5 hours is observed for the *25Ag/SiO₂* particles, which corresponds to 2 μg/ml of Ag content.

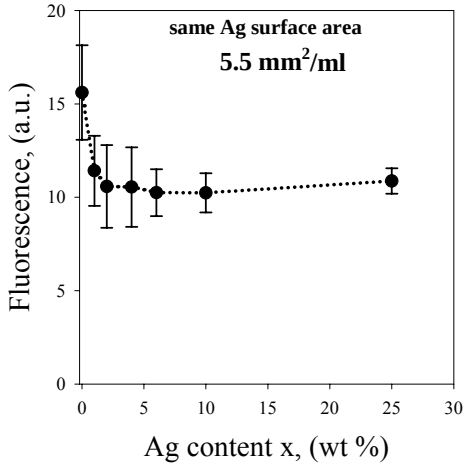

Figure 4: The final biomass after cultivation for 5.5 hours at 37 °C, in the presence of all the different Ag content particles on the basis of equivalent Ag surface area.

Taking into account the possible mechanisms responsible for the antibacterial activity of Ag nanoparticles, it is suggested that the *Ag* SSA_{EXP} plays an important role. In the case of the Ag's ability to damage vital compounds on the membrane or even compounds inside the cell, it is of highest importance to increase the contact of the Ag nanoparticles with these compounds, and thus to increase the *Ag* SSA_{EXP}. In the case of the Ag^+ ions being released from the Ag's surface, also the higher *Ag SSA*, the more Ag^+ ions would be released, making the Ag particles with the highest *Ag* SSA_{EXP} the most effective ones. Therefore, it is of major importance to control the *Ag* SSA_{EXP} of the Ag/SiO_2 nanoparticles, which could be incorporated in polymer matrixes and other composites or be deposited to surfaces, for an antibacterial use.

Figure 4 shows the final biomass after cultivation for 5.5 hours at 37°C in the presence of all the different Ag content particles. In these experiments, the total particle concentration has been normalized in respect to the *Ag* SSA_{EXP}. Therefore, all the data are in the presence of the same amount of *Ag* SSA_{EXP} (5.5 mm^2/ml) for all the samples, apart from the sample containing only SiO_2. It can be observed that for pure SiO_2, the final biomass is the same as if no particles are present (as observed from Fig. 3); however, the data from the nanoparticles containing Ag data have similar values, indicating that the antibacterial effect is identical in all cases. This leads to the conclusion that the mechanism responsible for the antibacterial activity is strongly surface area dependent.

4 CONCLUSIONS

Silver nanoparticles dispersed within amorphous silica have been synthesized using FSP. Different precursor solutions have been examined, and their effects on the final product particles have been investigated. Particle size and particle homogeneity can be tuned depending on the precursor solution. Additionally, the amount of the *Ag* SSA_{EXP} depends on the Ag precursor used. Higher values of *Ag* SSA_{EXP} were obtained for Ag precursors with higher decomposition point. The antibacterial activity of the produced nanoparticles was also investigated. There was a more enhanced antibacterial effect for an increased Ag content dose, in the presence of all the different particles. Finally, the strong dependency of the antibacterial activity on the exposed metallic surface area was demonstrated by monitoring the growth curves of the bacteria in the presence of the produced particles, on the basis of equivalent *Ag* SSA_{EXP} concentrations.

REFERENCES

[1] Q. L. Feng, J. Wu, G. Q. Chen, F. Z. Cui, T. N. Kim, J. O. Kim, *J. Biomed. Mater. Res.* **2000**, *52*, 662.

[2] J. R. Morones, J. L. Elechiguerra, A. Camacho, K. Holt, J. B. Kouri, J. T. Ramirez, M. J. Yacaman, *Nanotechnology* **2005**, *16*, 2346.

[3] C. N. Lok, C. M. Ho, R. Chen, Q. Y. He, W. Y. Yu, H. Sun, P. K. H. Tam, J. F. Chiu, C. M. Che, *J. Biol. Inorg. Chem.* **2007**, *12*, 527.

[4] C. Baker, A. Pradhan, L. Pakstis, D. J. Pochan, S. I. Shah, *Journal of Nanoscience and Nanotechnology* **2005**, *5*, 244.

[5] Y. Han, J. Jiang, S. S. Lee, J. Y. Ying, *Langmuir* **2008**, *24*, 5842.

[6] S. E. Pratsinis, *Prog. Energy Combust. Sci.* **1998**, *24*, 197.

[7] L. Madler, H. K. Kammler, R. Mueller, S. E. Pratsinis, *J. Aerosol. Sci.* **2002**, *33*, 369.

[8] M. J. Height, S. E. Pratsinis, O. Mekasuwandumrong, P. Praserthdam, *Appl. Catal. B-Environ.* **2006**, *63*, 305.

[9] S. Hannemann, J. D. Grunwaldt, F. Krumeich, P. Kappen, A. Baiker, *Appl. Surf. Sci.* **2006**, *252*, 7862.

[10] M. J. Height, S. E. Pratsinis, *Switzerland Patent*, **2007**.

[11] R. Jossen, S. E. Pratsinis, W. J. Stark, L. Madler, *J. Am. Ceram. Soc.* **2005**, *88*, 1388.

[12] J. Sambrook, D. W. Russell, *Molecular cloning: a laboratory manual*, Cold Spring Harbor, New York **2001**.

[13] S. Lambert, C. Cellier, P. Grange, J. P. Pirard, B. Heinrichs, *J. Catal.* **2004**, *221*, 335.